PROCEEDINGS of the
23rd International Congress on Acoustics
9 to 13 September 2019 in Aachen, Germany

Efficient numerical prediction and experimental validation of impact sound radiation by timber joist floors

Pengchao WANG(1), Cédric VAN HOORICKX(1), Geert LOMBAERT(1),Edwin REYNDERS(1)

(1)KU Leuven, Department of Civil Engineering, Kasteelpark Arenberg 40, 3001 Leuven, Belgium, pengchao.wang@kuleuven.be

Abstract

Timber joist floors are widely applied in residential buildings. The accurate impact sound radiation prediction of a bare timber joist floor is characterized by three main challenges. First, the prediction of the impact force on a timber joist floor is more difficult than that for a traditional heavyweight floor, since the low impedance of the timber joist floor induces more complex interaction between the excitation source and the floor. Second, the dynamic behavior of the floor is strongly affected by several characteristics, such as the finite dimensions, plate-joist coupling, orthotropic mechanical properties, boundary conditions, etc. Third, it is difficult to efficiently compute the precise acoustic field for the whole building acoustic frequency range. This work proposes a two-step numerical prediction model for impact sound radiation. First, the impact force of the ISO tapping machine is computed, considering the floor-hammer interaction. Second, the vibration field is accurately computed by a detailed finite element model of the floor, and the sound field in the room is subsequently computed by an efficient diffuse field model. This prediction model is experimentally validated in a case study of a timber joist floor. Differences between the measured and computed normalized impact sound pressure level according to ISO 717-2 did not exceed 2 dB.

Keywords: impact sound radiation, lightweight timber joist floor, ISO tapping machine, finite element method, diffuse field model

1 INTRODUCTION

The market share of timber joist floors in residential buildings has steadily increased in recent years [1]. However, it is challenging to achieve good impact sound insulation with a bare timber joist floor, due to its light weight [2]. The sound insulation of bare timber joist floors can be improved by adding components such as a floating screed or a suspended ceiling, as demonstrated in experimental studies [3]. Homb et al. [4] categorized timber joist configurations into different groups, and experimentally investigated the effects of various configurations on the impact sound insulation.

The efficient and cost-effective development and optimization of lightweight floor systems requires a computationally efficient and sufficiently accurate mathematical prediction of their impact sound radiation, because the experimental testing of a large number of alternative configurations is usually expensive and time-consuming. However, such a prediction generally needs to address several challenges, including the predictions of (i) the impact force, (ii) the vibration field of the timber joist floor, and (iii) the sound power radiated by the floor into a room.

The first challenge lies in the prediction of the impact force that is exerted onto the floor. Even for the standardized ISO tapping machine [5], predicting the impact force with sufficient accuracy is challenging because, in contrast to heavy floors, the interaction between the actuator and the lightweight timber joist floor cannot be neglected. Timoshenko and Goodier [6] investigated the local reaction of a rigid hammer excitation on an infinite plate, and derived expressions of local force mobility. Brunskog and Hammer [7] analyzed the hammer-floor interaction using a lumped mass-spring-dashpot model. However, the precise prediction of the ISO tapping machine impact force on a lightweight floor remains challenging. The impact force is for example determined by the hammer momentum change and the floor impedance [7, 8], which are generally difficult to quantify precisely.

The second challenge is predicting the vibration field of timber joist floors. Analytical solutions for the vi-

bration of lightweight periodical rib-stiffened plates have been provided, considering plate-joist coupling effects [9]. Since the amount of complexity that can be handled by analytical prediction models is limited, numerical approaches have also been presented. Kohrmann [1] constructed detailed finite element (FE) models to extensively analyze vibrations of various Cross-Laminated Timber (CLT) plates with lumber joists, hollow box girders, floating floors, and suspended ceilings. Paolini et al. [10] developed a high-order FE model of a CLT structure, and the unknown model parameters were determined by matching simulated and measured modal results in a model calibration process. Nevertheless, also the predictive accuracy of the numerical models heavily depends on the accuracy of the dynamic material properties of the floor components, and on whether the assumptions regarding the connections between the different components and the boundary conditions are realistic or not.

The third challenge, i.e., the prediction of the sound power that is radiated by the floor into the receiving room, requires the consideration of different frequency regimes. Neves e Sousa and Gibbs [11] developed an analytical model to compute the acoustic response in the room under a point-loaded floor at low frequencies. They highlighted the effects of floor-room modal coupling on the acoustic response. Bard et al. [12] analyzed the pressure field in the receiving room using a basis of analytical solutions of the Helmholtz equation. At medium and high frequencies, the sound field in the room is usually modeled as diffuse [13]. Rayleigh integral is typically available to numerically evaluate the radiated sound power [14].

The aim of the this work is to investigate to which degree of accuracy the impact sound insulation of timber joist floors can be predicted with currently available, computationally efficient state-of-the-art approaches. A practical numerical model is elaborated in this work for the prediction of impact forces, structural vibrations and impact sound radiation. A case study of a timber joist floor is presented, in which the numerical model is experimentally validated.

The outline of the paper is as follows. Section 2 introduces the proposed numerical prediction model for impact sound radiation prediction of timber joist floors. Section 3 performs an experimental validation of the numerical model in a case study of a timber joist floor. Finally, section 4 concludes the work.

2 NUMERICAL PREDICTION MODEL

This section presents a two-step numerical prediction model for impact sound radiation by a lightweight timber joist floor. First, in section 2.1, the impact force of the ISO tapping machine is computed using the mass-impedance model proposed by Brunskog and Hammer [7]. In the second step, the structural response of the floor and sound pressure levels in the underlying room are subsequently computed by a FE-diffuse field model, as given in section 2.2.

2.1 ISO tapping machine impact force

As commonly assumed, the tapping machine is modeled as a point excitation source with an impact period $T_0 = 0.1\,\mathrm{s}$. Figure 1 shows a model for the tapping machine excitation at an angular frequency ω_n, with $n \in \mathbb{Z}$. The hammer is described by its mass $m_\mathrm{h} = 0.50\,\mathrm{kg}$ and a blocked force with an amplitude of $\hat{f}_{\mathrm{bl},n}$. Using the momentum-impulse theorem, the blocked force is given by [8]

$$\hat{f}_{\mathrm{bl},n} = m_\mathrm{h} \Delta v / T_0 = m_\mathrm{h} \Delta v f_0 \tag{1}$$

where $f_0 = 1/T_0 = 10\,\mathrm{Hz}$ is the impact frequency, and Δv is the hammer velocity change during an impact. Δv equals v_0 and $2v_0$ for perfectly plastic and elastic collisions, respectively. An assumption is often made based on the type of floor; alternatively, it is numerically approximated [7, 8].

As shown in Figure 1, the driving point impedance Z_dp consists of a local part Z_L and a global part Z_G, representing the resistance to local deformation at the hammer-floor contact surface, and the resistance to global floor motion, respectively. For periodical excitation of the hammer, the impact force in the frequency domain is

written as Fourier series coefficients:

$$\hat{f}_{\mathrm{imp},n} = \frac{\hat{f}_{\mathrm{bl},n}}{1+\mathrm{i}\omega_n m_\mathrm{h}/Z_\mathrm{dp}} = \frac{m_\mathrm{h}\Delta v f_0}{1+\mathrm{i}\omega_n m_\mathrm{h}(Z_\mathrm{G}+Z_\mathrm{L})/(Z_\mathrm{G}Z_\mathrm{L})} \tag{2}$$

The global impedance Z_G for a finite floor is complex, with its real and imaginary part representing the energy dissipating part and stiffness part, respectively. In this work, the global impedance Z_G is computed using the detailed FE model of the floor presented in section 3. On the other hand, the local impedance Z_L is analytically computed using Timoshenko and Goodier's approach [6]:

$$Z_\mathrm{L} = \frac{2Er_\mathrm{h}}{\mathrm{i}\omega(1+\nu)(1-\nu)} \tag{3}$$

where E and ν are the Young's modulus and Poisson's ratio for isotropic floor materials, and $r_\mathrm{h} = 1.5\,\mathrm{cm}$ is the radius of the tapping machine hammer.

2.2 Impact sound radiation

This section describes a FE-diffuse field model to compute the structural vibration of the floor and resulting impact sound pressure level in the underlying room. The structural vibration is predicted by a fully detailed FE model of the floor. The sound field in the room is regarded as a combination of a direct field and a diffuse field, such that the radiated sound power flows into the direct field, and then is reflected and dissipated at the random boundaries of the diffuse field. The diffuse field model is computationally efficient, and its predictive accuracy is satisfactory at middle and high frequencies.

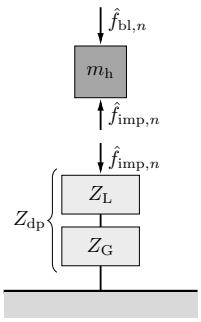

Figure 1. Model for the ISO tapping machine hammer excitation on a floor.

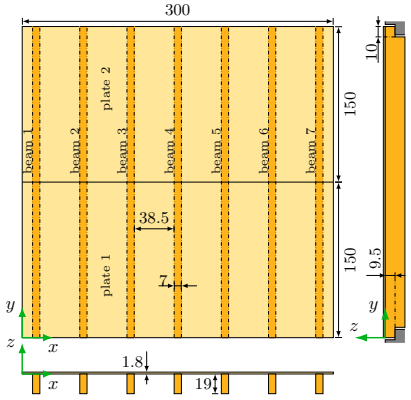

Figure 2. Top, front, and side view of the timber floor. The dimensions are in [cm].

At an angular frequency ω, the structural displacement at an arbitrary coordinate $\mathbf{x}$ due to an excitation at the coordinate $\mathbf{x}_0$ is computed using modal decomposition:

$$\hat{u}(\omega,\mathbf{x}) = \sum_{j=1}^{n_\mathrm{m}} \frac{\phi_j(\mathbf{x})\phi_j(\mathbf{x}_0)\hat{f}(\mathbf{x}_0)}{-\omega^2+\omega_j^2+\mathrm{i}\eta_\mathrm{s}\omega\omega_j} \tag{4}$$

where $\hat{f}(\mathbf{x}_0)$ is the impact force at the coordinate $\mathbf{x}_0$, $\phi_j(\mathbf{x})$ and ω_j are the mode shape at the coordinate $\mathbf{x}$ and angular natural frequency of the structural mode j, n_m is the number of structural modes that are considered to contribute to the structural response, and η_s is the structural damping loss factor. Next, the sound power radiated by the infinitely baffled floor into the direct field is computed by

$$\hat{P}_\mathrm{rad} = (\omega/2)\mathrm{Im}\{\hat{\mathbf{u}}^\mathrm{H}(\omega)\mathbf{D}_\mathrm{dir}\hat{\mathbf{u}}(\omega)\} \tag{5}$$

in which $\hat{\mathbf{u}} \in \mathbb{C}^{n_{\text{dof}}}$ is the displacement vector, with n_{dof} the number of structural DOFs along the floor-room interface. $\mathbf{D}_{\text{dir}} \in \mathbb{C}^{n_{\text{dof}} \times n_{\text{dof}}}$ is the dynamic stiffness matrix of the direct field, as seen from the floor-room interface [17]. The notation $(\cdot)^{\text{H}}$ denotes the Hermitian transpose, i.e., $\hat{\mathbf{u}}^{\text{H}} = \hat{\mathbf{u}}^{*\text{T}}$. Next, the radiated power $\hat{P}_{\text{rad}}$ is dissipated in the diffuse field of the room:

$$\hat{P}_{\text{rad}} = \hat{P}_{\text{diss}} \tag{6}$$

in which the dissipated power $\hat{P}_{\text{diss}}$ is computed by [18]

$$\hat{P}_{\text{diss}} = \omega \eta_{\text{a}} \hat{E}_{\text{a}} \tag{7}$$

where $\hat{E}_{\text{a}}$ is the sound energy averaged over an ensemble of rooms with the same volume V and acoustic damping loss factor η_{a}, but with random wave scattering in the room and at its boundaries. The ensemble mean of the sound energy $\hat{E}_{\text{a}}$ is easily computed using equations (5) to (7). The normalized impact sound pressure level in the receiving room equals

$$\hat{L}_{\text{n}} = 10\log\left(\hat{E}_{\text{a}} \rho_0 c^2 / (V p_0^2)\right) + 10\log(A/A_0) \tag{8}$$

where c is the sound speed in air, ρ_0 is the air density, $p_0 = 2 \times 10^{-5}\,\text{Pa}$, and $A_0 = 10\,\text{m}^2$ are the reference sound pressure and the reference absorption area, respectively.

3 IMPACT SOUND PREDICTION AND EXPERIMENTAL VALIDATION

In this section, the numerical model presented in the previous section is experimentally validated in the following case study of a timber joist floor. Section 3.1 describes the considered floor. Section 3.2 illustrates the FE model of the floor. Section 3.3 describes the measurement setups of an impact sound radiation test, an acoustic reverberation test, and a structural reverberation test. Section 3.4 discusses the experimental validation of the computed sound pressure levels for the ISO tapping machine excitation.

3.1 Description of the timber joist floor

Figure 2 shows the top, front, and side view of the considered lightweight timber joist floor, which is assembled in a $3\,\text{m} \times 3\,\text{m}$ opening in the KU Leuven Laboratory of Acoustics. The receiving room below the floor has a volume of $V = 87\,\text{m}^3$. The floor consists of two timber plates supported by a total of seven joist beams. Each plate has nominal dimensions of $3\,\text{m} \times 1.5\,\text{m} \times 0.018\,\text{m}$, and consists of seven thin timber layers. The fiber orientations of two adjacent thin layers are orthogonal. Each beam has nominal dimensions of $3\,\text{m} \times 0.07\,\text{m} \times 0.19\,\text{m}$, and is connected with the two plates by ten screws along the central longitudinal axis of the beam.

The floor components are assumed to be homogeneous, despite the inhomogeneous nature of the wooden texture. Table 1 lists the densities ρ of the floor components, the Young's moduli E_{x} and E_{y} of the seven beams, and the Young's moduli E_{x} and E_{y}, the major Poisson's ratio ν_{xy}, and the shear modulus G_{xy} of two plates. The stiffness parameters in table 1 were systematically calibrated using the experimentally determined eigenmodes of separate floor components. The stiffness parameters of floor components that are not shown in table 1 were either assumed according to [19], or computed from the determined parameters [20].

3.2 FE model of the floor

Figure 3 shows the FE model of the floor, which is assembled from the seven beam models and two plate models, respectively. The beams and plates were constructed in ANSYS with 3D eight-node linear solid elements (of the SOLID45 type) of size $2.0\,\text{cm} \times 2.0\,\text{cm} \times 2.0\,\text{cm}$, and with four-node linear thin shell elements (of the SHELL181 type) of size $2.5\,\text{cm} \times 2.5\,\text{cm}$, respectively. The neutral plane of the two plates is 9 mm higher than the top surfaces of the beams. It is assumed that, at a screw point, the plate is strongly coupled to the beam, such that the plate and the beam are vibrating without any relative translation or rotation. To achieve such a plate-beam connection through the screw, all translational DOFs of the plate within a radius of 4 cm to the screw are coupled to the closest translational DOF of the beam.

Component	plate		beam						
No.	1	2	1	2	3	4	5	6	7
ρ [kg/m^3]	515	535	489	511	593	561	484	524	534
E_x [GPa]	5.24	4.96	0.21	0.19	0.28	0.25	0.21	0.18	0.17
E_y [GPa]	4.53	5.06	13.99	13.42	16.28	15.33	14.02	15.06	14.84
G_{xy} [GPa]	0.30	0.33							
ν_{xy} [−]	0.31	0.31							

Table 1. Densities and calibrated stiffness parameters of the floor components.

It was assumed that some beam ends were lifted from their support when screwing the plates onto the beams. Following this assumption, the boundary conditions were investigated by evaluating the effect of each beam end on the modal characteristics. The boundary conditions were finally specified by keeping four beam ends free, while constraining the vertical translational DOFs at the other beam ends. These boundary conditions achieve better correspondences between the measured and computed modal characteristics than other ones that had been investigated.

3.3 Measurement setup

An impact sound radiation test was performed, consisting of 16 setups. In eight setups, the ISO tapping machine was placed above a beam, and in the other eight setups, the machine was placed at midspan between two beams. In each setup, the sound pressure level was measured at eight microphone positions in the central zone of the receiving room.

An acoustic reverberation test was performed, and the acoustic reverberation time T_a in the receiving room was evaluated using the interrupted noise method as standardized in ISO-3382 [21]. The acoustic damping loss factor η_a at angular frequency ω was computed by

$$\eta_a = 4.4\pi/(\omega T_a) \tag{9}$$

Analogously, a structural reverberation test was performed, and the structural reverberation time T_s was evaluated using the integrated impulse response method as standardized in ISO-3382 [21]. Next, the structure damping loss factor η_s at angular frequency ω was computed as follows:

$$\eta_s = 4.4\pi/(\omega T_s) \tag{10}$$

Figure 2 shows the measured acoustic reverberation time T_a of the receiving room and the damping loss factor η_s of the floor.

f [Hz]	63	125	250	500	1000	2000	4000
T_a [s]	2.18	1.16	1.03	1.31	1.52	1.49	1.27
η_s [%]	3.70	2.32	2.21	1.47	2.31	2.18	1.59

Table 2. Measured reverberation time T_a of the receiving room and the damping loss factor η_s of the floor.

3.4 Validation for tapping machine excitation

The ISO tapping machine impact force is computed using the approach in section 2.1. in which the hammer excitation on the timber floor is assumed as a perfectly plastic collision. Figure 4 shows the computed equivalent power spectra densities of the ISO tapping machine impact force. At frequencies below 100 Hz, the magnitudes of the impact force spectra are controlled by the floor stiffness, and are close to the pseudo force spectra. For frequencies between 100 Hz and 1000 Hz, the results for excitation on top of a beam are different from the ones

for excitation between beams. This is mainly due to the considerable difference of the point impedances at beam and inter-beam positions. For excitation on top of a beam, a resonance peak appears at 550 Hz, corresponding to the mass-spring resonance that is determined by the hammer mass and driving point stiffness. At frequencies above 1000 Hz, the impact force spectra are controlled by the hammer mass.

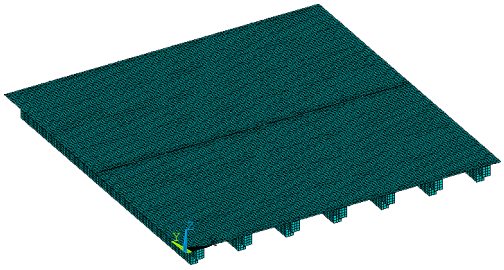

Figure 3. FE model of the assembled floor in ANSYS.

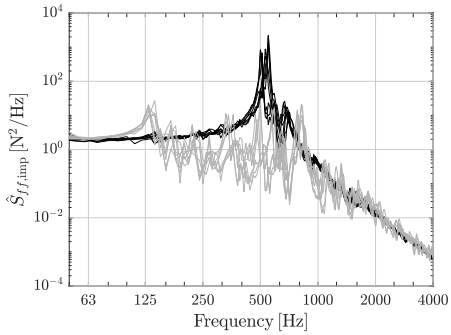

Figure 4. Computed power spectra densities of squared impact force spectra of excitations on eight beam positions (black solid line) and eight inter-beam positions (gray solid line) in the sound radiation test.

Figure 5 shows the measured and computed normalized sound pressure levels in the receiving room that are integrated over 1/48-octave bands and 1/3-octave bands, and averaged over eight beam positions and eight inter-beam positions of the tapping machine, respectively. In general, the measured and computed sound pressure levels have a similar order of magnitudes. The discrepancies between the measured and computed 1/48-octave band integrated results are attributed to the moderate accuracies of the FE model of the floor, the estimated structural and acoustic damping loss factors, and the measurement errors. The discrepancies at low frequencies are also attributed to acoustic resonances, which are not considered in the diffuse room model, but influence the acoustic response in this frequency range. Furthermore, the impact force of the tapping machine was computed using the assumptions in section 2.1, resulting in additional model errors.

The correspondence between the measurements and computations is further evaluated by comparing single number ratings in accordance with ISO-717-2-1996 [22]. The plots in Figure 5(c-f) show the single number rating values in the form of $L_{\mathrm{n,w}}(C_{\mathrm{I}})$, for the measured and computed normalized sound pressure levels integrated in 1/3-octave bands. For both the beam and inter-beam excitation, the computed single number rating differs only $0-2$ dB from the measured one. Therefore, the numerical model given in section 2 gives a good prediction of sound radiation induced by the ISO tapping machine.

4 CONCLUSION

This work proposes a two-step numerical prediction model for impact sound radiation by timber joist floors. First, the impact force of the ISO tapping machine is computed using both the local and global impedance of the driving point, and the latter is determined from a detailed FE model of the floor. Second, the structural vibration and radiated sound power are computed using an FE-diffuse field model, which is both computationally efficient and accurate at middle and high frequencies. This prediction model is experimentally validated in a case study of a timber joist floor. Differences between the measured and computed normalized impact sound pressure level according to ISO 717-2 did not exceed 2 dB.

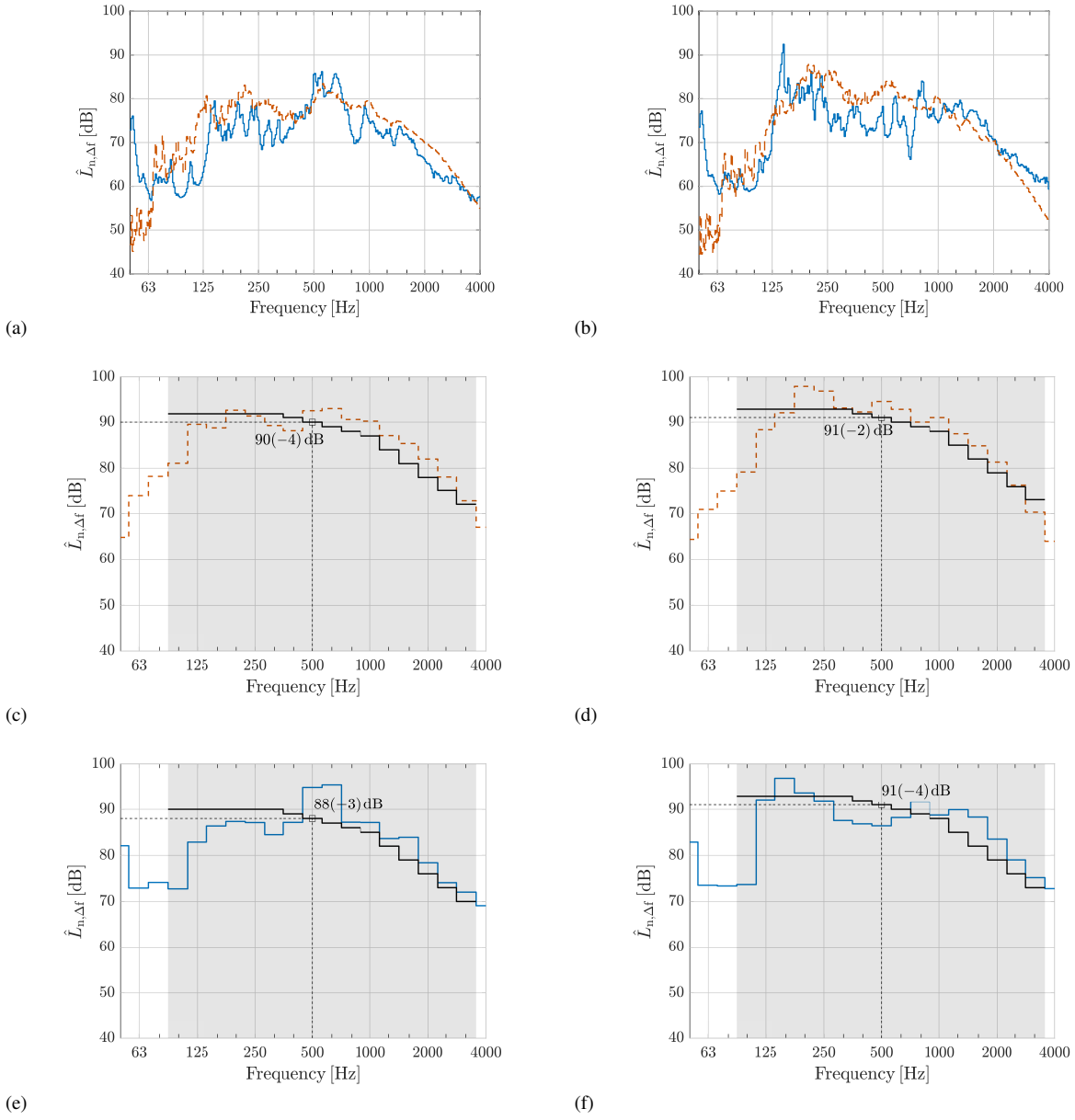

Figure 5. Measured (red dashed line) and computed (blue solid line) normalized sound pressure levels in the receiving room integrated over (a,b) 1/48-octave bands and (c-f) 1/3-octave bands, and averaged over tapping machine excitations at (a,c,e) eight beam positions and (b,d,f) eight inter-beam positions of the floor. The measured results are also averaged over the microphone positions in the room. Plots (c-f) additionally display shifted reference curves (black) and single number rating values $L_{n,w}(C_I)$ in accordance with ISO-717-2-1996. The gray zones indicate the frequency range for single number ratings.

Acknowledgments

This research was funded by the European Research Council (ERC) Executive Agency, in the form of an ERC Starting Grant under the Horizon 2020 framework program, project 714591 VirBAcous, and by the KU Leuven

Dept. of Civil Engineering. The financial support from the European Commission and from KU Leuven is gratefully acknowledged. The authors would also like to thank Jan Van den Wyngaert for his help with the impact sound radiation measurement, and Bernd Salaets, Jimmy Van Criekingen, and Willy Bruyninckx for their contribution in the installation of the timber joist floor.

References

[1] Kohrmann, M. Numerical methods for the vibro-acoustic assessment of timber floor constructions. PhD thesis, Technical University Munich, 2017.

[2] Negreira, J. Vibrations in lightweight buildigns - preception and prediction. PhD thesis, Lund University, 2013.

[3] Ingelaere, B. COST Action: Net-acoustics for timber based lightweight buildings and elements - Chapter 4: acoustic design of lightweight timber frame constructions. FP0702, BBRI, Brussels, 2012.

[4] Homb, A.; Guigou-Carter, C.; Hagberg, K.; Schmid, H. Impact sound insulation of wooden joist constructions: collection of laboratory measurements and trend analysis. Build. Acoust., Vol 23(2), 2016, pp 73-91.

[5] International Organization for Standardization. ISO 10140-5: Acoustics - Laboratory measurement of sound insulation of building elements - Part 5: Requirements for test facilities and equipment, 2010.

[6] Timoshenko, S.P.; Goodier, J.N. Theory of elasticity. McGraw-Hill, 3rd edition, 1970.

[7] Brunskog, J.; Hammer. P. The interaction between the iso tapping machine and lightweight floors. Acta Acust united Ac., Vol 89(2), 2003, pp 296-308.

[8] Wittstock, V. On the spectral shape of the sound generated by standard tapping machines. Acta Acust united Ac., Vol 98, 2012, pp 301-308.

[9] Brunskog, J.; Hammer. P. Prediction model for the impact sound level of lightweight floors. Acta Acust united Ac., Vol 89(2), 2003, pp 309-322.

[10] Paolini, A.; Kollmannsberger, S.; Winter, C.; Buchschmid, M.; Müller, G.; Rabold, A.; Mecking, S.; Schanda, U.; Rank, E. A high-order finite element model for vibration analysis of cross-laminated timber assemblies. Build. Acoust., Vol 24(3), 2017, pp 135-158.

[11] Neves e Sousa, A.; Gibbs, B.M. Low frequency impact sound transmission in dwellings through homogeneous concrete floors and floating floors. Appl Acoust., Vol 72(4), 2011, pp 177-189.

[12] Bard, D.; Negreira, J.; Guigou-Carter, C.; Borello, G.; Kouyoumji, J.; Speranza, A.; Coguenanff, C.; Hagberg, K. Modelling prerequisites - fem/sea impact and airborne sound. Report 56, RISE Research Institutes of Sweden AB, 2017.

[13] Hopkins, C. Sound insulation. Elsevier Ltd., Oxford, 2007.

[14] Cremer, L.; Heckl, M.;Petersson, B.A.T. Structure-borne sound: Structural vibrations and sound radiation at audio frequencies. Springer, Berlin, 3rd edition, 2005.

[15] Vér, I.L. Impact noise isolation of composite floors. J. Acoust. Soc. Am., Vol 50(4), 1971, pp 1043-1050.

[16] Langley, R.S.; Bremner, P. A hybrid method for the vibration analysis of complex structural-acoustic systems. J. Acoust. Soc. Am., Vol 105(3), 1999, pp 1657-1671.

[17] Langley, R.S.; Cotoni, V. Response variance prediction for uncertain vibro-acoustic systems using a hybrid deterministic-statistical method. J. Acoust. Soc. Am., Vol 122(6), 2007, pp 3445-3463.

[18] Langley, R.S.; Cordioli, J.A. Hybrid deterministic-statistic analysis of vibro-acoustic systems with domain couplings on statistical components. J Sound Vib, Vol 321(3-5), 2009, pp 893-912.

[19] Ross, R. Wood handbook: wood as an engineering material. Technical Report 190, USDA Forest Service, Forest Products Laboratory, 2010.

[20] Huber, M. The theory of crosswise reinforced ferroconcrete slabs and its application to various important constructional problems involving rectangular slabs. Der Bauingenieur, Vol 4(23), 1923, pp 354-360.

[21] International Organization for Standardization. ISO-3382: Acoustics - Measurement of the reverberation time of rooms with reference to other acoustical parameters, 1997.

[22] International Organization for Standardization. ISO 717-2: Acoustics - Rating of sound insulation in buildings and of building elements - Part 2: Impact sound insulation, 1996.